Superthermal electron distribution measurements from polarized electron cyclotron emission (invited)

T. C. Luce,[a] P. C. Efthimion, and N. J. Fisch

Plasma Physics Laboratory, Princeton University, Princeton, New Jersey 08544

(Presented on 15 March 1988)

Measurements of the superthermal electron distribution can be made by observing the polarized electron cyclotron emission. The emission is viewed along a constant magnetic field surface. This simplifies the resonance condition and gives a direct correlation between emission frequency and kinetic energy of the emitting electron. A transformation technique is formulated which determines the anisotropy of the distribution and number density of superthermals at each energy measured. The steady-state distribution during lower hybrid current drive and examples of the superthermal dynamics as the runaway condition is varied are presented for discharges in the PLT tokamak.

INTRODUCTION

The advent of noninductive current drive[1] and intense-pulse heating schemes[2] has generated a great deal of interest in the measurement of superthermal electron distributions. Determination of the distribution function is a much more stringent test of microscopic theories than global measurements such as efficiency or parameter scaling. Previous attempts to infer the distribution function from electron cyclotron emission (ECE) centered on varying the parameters of analytic fitting functions.[3–6] In certain cases, a transformation analysis was applied to the data.[6,7] We present a more general transformation technique which provides information on the anisotropy and number density of superthermal electrons from the measurement of the ECE frequency spectra of both polarizations. As a demonstration of the technique, examples are given of superthermal distributions and their temporal evolution for lower hybrid current drive (LHCD) and runaway discharges on the PLT tokamak.

I. EXPERIMENTAL ARRANGEMENT

The main reason ECE is useful for determining the distribution function is that it is a resonance phenomenon—an electron with a given momentum emits radiation at a discrete set of frequencies. This is in contrast to x-ray bremsstrahlung, where an electron can emit photons of any energy up to its entire kinetic energy. The general resonance condition for ECE is[8]

$$\omega = \frac{nqB(\mathbf{r})}{\gamma m_0 c} \frac{1}{1-\beta_{\parallel}\cos\theta}, \tag{1}$$

where ω is the emission frequency, n is the harmonic number (an integer $\geqslant 1$), γ is the standard relativistic factor $(1-\beta^2)^{-1/2}$, $\beta_{\parallel}$ is the electron velocity parallel to the magnetic field, and θ is the angle between the direction of emission and the magnetic field direction. For the case of an inhomogeneous magnetic field which varies on a scale length much larger than the electron gyroradius $p_{\perp}/m_0\omega_0$, the only change in Eq. (1) is $B = B(\mathbf{r})$. At each harmonic, there are three effects which lead to variations in the emission frequency: the magnetic field inhomogeneity alters the local rest-mass cyclotron frequency $\omega_0 = eB/m_0c$, the relativistic mass increase lowers the actual cyclotron frequency $\omega_c = \omega_0/\gamma$ as the energy $\gamma m_0 c^2$ increases, and the Doppler shift caused by relative motion in the parallel direction between the emitting electron and the observer shifts the frequency by $\beta_{\parallel}\cos\theta$.

We have chosen an experimental arrangement, shown in Fig. 1, which reduces the resonance condition to a much simpler form for the case of a low-beta tokamak. Observing emission along a chord perpendicular to the magnetic field minimizes the frequency shift due to the Doppler effect. Some Doppler broadening remains due to divergence of the antenna pattern. It should be noted that this choice of viewing angle eliminates all information about the direction of the parallel velocity. For runaway discharges and the lower hybrid current drive experiments on PLT, this restriction caused little difficulty since the superthermal distributions were expected to be one sided. The most important choice in the viewing arrangement is to observe emission along a chord where the magnetic field is constant. For all present tokamaks, a vertical line of sight is along a surface of constant toroidal field. The poloidal field and diamagnetic effects alter the magnitude of the magnetic field by less than 1% for PLT parameters. Here again there will be some residual frequency broadening due to the variation in the toroidal field across the antenna pattern. The resonance condition [Eq. (1)] is reduced to the simple form $\omega = n\omega_0/\gamma$, where ω_0 is a constant, ignoring the nonideal antenna pattern effects for the moment. This condition implies that, given the harmonic number, there is a one-to-one correspondence

 0034-6748/88/081593-06$01.30

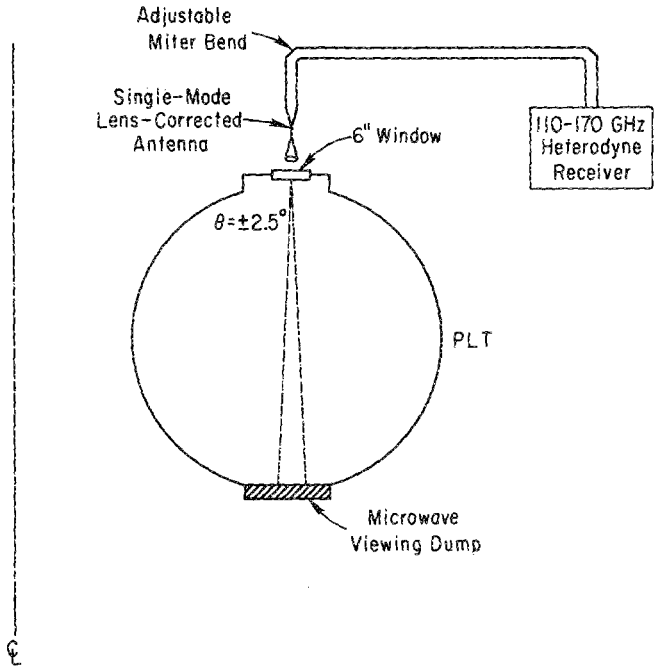

FIG. 1. Schematic of the experimental arrangement on PLT.

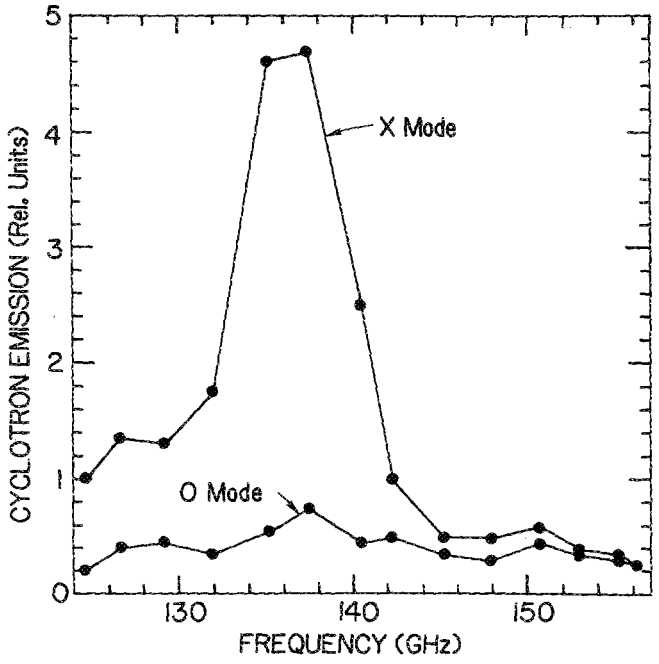

FIG. 2. Thermal linewidths for the X and O modes.

between the emission frequency and the kinetic energy of the emitting electron. Therefore, any frequency broadening limits the energy resolution.

The beam divergence angle and the width of the antenna pattern at the plasma center determine the energy resolution of the diagnostic. Laboratory measurements of the antenna pattern indicate that the beam divergence is 2.5° at the 6-dB points, giving a beam radius of 2.5 cm at the plasma center. Ray tracing indicates that plasma refraction is not important for densities near 1.0×10^{13} cm^{-3}. For the simple resonance condition, $|\Delta\omega|/\omega = |\Delta\gamma|/\gamma$; the resolution of the kinetic energy is $|\Delta E_k|/E_k = |\Delta\gamma|/(\gamma-1) = (|\Delta\omega|/\omega)\gamma/(\gamma-1)$. For the broadening due to the toroidal field variation, $|\Delta\omega|/\omega = |\Delta R|/R \simeq 1.9\%$. This gives an energy resolution $|\Delta E_k|/E_k \sim 8\%$ for the lowest values of γ measured. For the Doppler broadening, $|\Delta\omega|/\omega \simeq 2.8\%$, which gives $|\Delta E_k|/E_k \sim 12\%$. These estimates of the resolution are for the worst cases (small γ).

The discussion above assumes that all of the emission comes from direct emission into the antenna. A viewing dump inside the vacuum vessel prevents the reflection of Doppler-shifted radiation and radiation from regions of different magnetic field into the antenna pattern and preserves the wave polarization. The dump was fabricated from Macor because of its low reflectivity in this frequency range.[9] Grooves were machined in the Macor block in two orthogonal directions with a 60° opening. The depth of the grooves was set to ensure at least a ten-wavelength opening width for the longest wavelengths measured. This design predicted a 2.5% reflectivity; bench tests indicated $<3\%$ reflectivity. The size of the viewing dump as installed was 15×25 cm, with the long dimension in the poloidal direction. An experimental verification that the dump eliminates the unwanted reflections is shown in Fig. 2. The toroidal field was selected so the second-harmonic thermal resonance was in the operational bandwidth of the receiver. Shown are spectra of the extraordinary (X) and ordinary (O) mode polarizations at one time slice. If the dump functions properly and there are no superthermals present, only emission corresponding to thermal cyclotron emission in the line of sight should be seen. The linewidth is then indicative of the inherent frequency resolution of the instrument. The measured linewidth of $\pm 3\%$ is consistent with the broadening mechanisms discussed above. If the antenna did not view the dump or the dump were reflective, emission would appear across the entire band at nearly the same level for both polarizations due to reflections and polarization scrambling. The slight asymmetry in the X mode is attributed to a small population of runaways ($n_{st} < 10^9$ cm^{-3}). The peak of the X-mode spectra was clipped by the instrument, so the X/O ratio is only known to be >7. This ratio is consistent with the X mode becoming optically thick in the outer region of the plasma and the O mode viewing the center with an optical depth $\tau \simeq 0.2$.

To detect the emission, a swept heterodyne radiometer in the frequency range 110–170 GHz was constructed. A block diagram of the receiver is shown in Fig. 3. The details of this type of receiver have been discussed elsewhere.[10,11] The frequency range of 115–160 GHz can be swept every 5 ms by changing the voltage on the backward-wave oscillator tube which serves as the local oscillator. This frequency range lies between the first and second thermal cyclotron harmonics for the typical toroidal field strength on PLT (30 kG). The instrument can also be run in single-frequency mode with a time resolution of 50 μs. The signal-to-noise ratio was typically >100 for LHCD discharges. The receiver was calibrated against a blackbody at liquid-nitrogen temperature (77 K) at 32 frequencies for both polarizations.

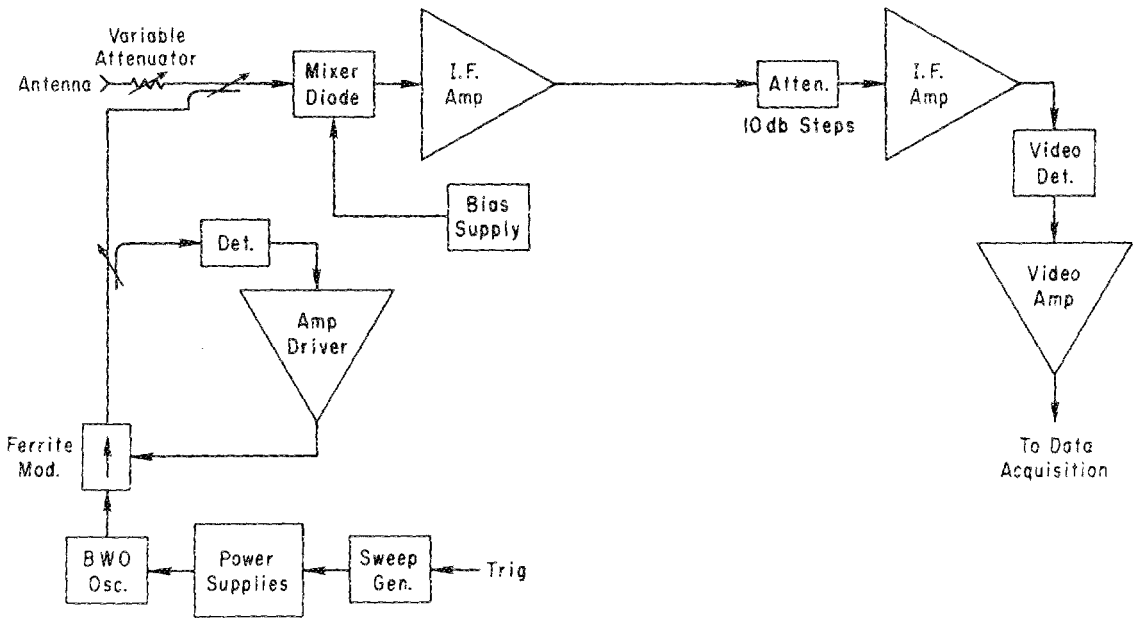

FIG. 3. Block diagram of the heterodyne receiver.

The calibration included the overmoded waveguide shown in Fig. 1, which has a total length of ~8 m. The calibration factors were typically in the range of 100 keV/V.

II. ANALYSIS TECHNIQUE

The choice of receiver strongly influences the mode of analysis. Previous experiments have used a Michelson interferometer to measure the vertical ECE between the first and third thermal cyclotron harmonics.[5–7] Since the cyclotron harmonics are mathematically independent, the Michelson interferometer can make two independent measurements of the distribution with the same discharge. The disadvantages of the Michelson are time and frequency resolution, which are intrinsically poorer than the heterodyne radiometer. Also, there is no possibility of single-frequency operation. The better time and energy resolution of the radiometer are gained at the expense of a much smaller operational bandwidth. This smaller bandwidth precludes using multiple harmonics as independent measurements. The alternative is to use the two orthogonal polarizations of the ECE, which are also mathematically independent. Both polarizations were measured with one instrument by operating reproducible discharges. The electron density, plasma current, loop voltage, and hard-x-ray bremsstrahlung signals indicated that the PLT tokamak would produce reproducible discharges over several hours.

Typical calibrated O- and X-mode data from a steady-state LHCD discharge are shown in Fig. 4. The second-harmonic thermal cyclotron resonance is at 170.7 GHz, which is above the measured range of frequencies. The error bars indicate the statistical error introduced in the calibration procedure. The superthermal ECE is well described by the single-particle emission theory[8] since dielectric effects are small. It is also assumed that reabsorption is negligible. For the simple resonance condition $\omega = n\omega_0/\gamma$, it is easy to show that the power emitted per solid angle per bandwidth per volume is reduced to the one-dimensional integrals

$$j_n^{(X)} = \frac{q^2\omega}{c} p_n^3 \int_{-1}^{1} dy(1-y^2) \times J_n'^2\left(\frac{\omega}{\omega_0} p_n (1-y^2)^{1/2}\right) f(p_n, y), \quad (2)$$

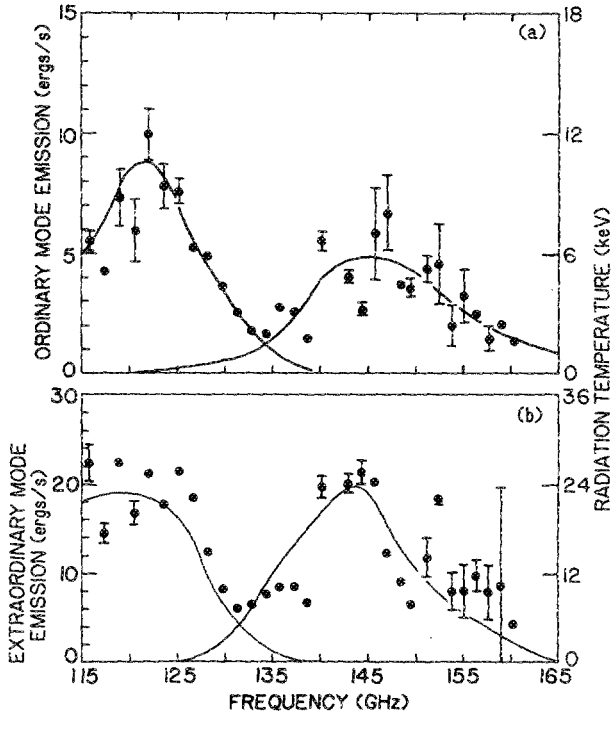

FIG. 4. Calibrated spectra for the (a) O mode and (b) X mode during a steady-state LHCD discharge. The lines drawn illustrate the decomposition of the emission into harmonics and are not a fit to the data.

$$j_n^{(O)} = \frac{q^2\omega}{c} p_n^3 \int_{-1}^{1} dy\, y^2 \times J_n^2\left(\frac{\omega}{\omega_0} p_n (1-y^2)^{1/2}\right) f(p_n, y), \quad (3)$$

where p_n is the resonant momentum normalized to m_0c, J_n and J_n' are the Bessel functions of the first kind of order n and its derivative with respect to the argument, y is the cosine of the pitch angle, and f is the distribution function.

To relate the X- and O-mode emission back to the superthermal distribution function, a transformation technique was developed. A transformation is preferable to parameter-fitting techniques because information about the distribution is gained without losing any of the information contained in the original data. The first transformation is from frequency to momentum by the resonance condition $\omega = n\omega_0/(1+p_n^2)^{1/2}$. The critical assumption is that the emission at any frequency can be attributed to a single harmonic. The lines drawn through the spectra in Fig. 4 illustrate the assignment of harmonics for the LHCD case. The spectra from the steady-state portion of these discharges always have the two-peak structure indicated in the figure. Spectra from Fokker–Planck simulations and fitting functions indicate that the peak at low frequency is predominantly second-harmonic emission while the high-frequency peak is predominantly third-harmonic emission. Therefore, $n = 2$ is assumed for emission below 129 GHz and $n = 3$ for emission above 135 GHz. The emission between 129 and 135 GHz is omitted from the analysis, since it consists of some unknown combination of the two harmonics. The peaking of the second-harmonic emission at $\gamma \simeq 1.4$ and the third-harmonic emission at $\gamma \simeq 1.7$ is consistent with the fact that the higher-harmonic emission should peak at larger values of γ.[8]

There are still two independent measurements at each frequency which can be related to the distribution function. For transformation variables, one is chosen which measures the anisotropy of the distribution at each energy and the other measures the density of electrons needed to reproduce the observed emission level. The transformation is taken to be in the form of a distribution $f(p_n, y)$ so that Eqs. (2) and (3) can be evaluated to model the emission. A distribution of the form

$$f(p_n, y) = \frac{\rho}{2\pi p_n^2} \delta(p - p_n)\delta(y - y_n) \quad (4)$$

is chosen, where ρ and y_n are the variables to which the X- and O-mode emission are transformed. Equations (2) and (3) then take on the simple form

$$j_n^{(X)} = \rho \frac{q^2\omega}{2\pi c} p_n (1-y_n^2) J_n'^2\left(\frac{\omega}{\omega_0} p_n (1-y_n^2)^{1/2}\right), \quad (5)$$

$$j_n^{(O)} = \rho \frac{q^2\omega}{2\pi c} p_n\, y_n^2 J_n^2\left(\frac{\omega}{\omega_0} p_n (1-y_n^2)^{1/2}\right). \quad (6)$$

The value of y_n is found numerically by matching the ratio $j_n^{(X)}/j_n^{(O)}$ to the measured polarization ratio. The conceptual interpretation of y_n is fairly simple. Since the assumption that the distribution is one sided is good in the cases of interest here, the distribution at a given energy lies almost entirely between $y = 0$ and $y = 1$. Now imagine shrinking the allowed range of pitch angles with the constraint that the polarization ratio remains at the measured value. The limiting value of pitch angle as the allowed range of pitch angles goes to 0 corresponds precisely to the pitch angle indicated by y_n. This is not mathematically equivalent to the average pitch angle, so we call $\cos^{-1} y_n$ the emission-weighted average pitch angle. That y_n is a measure of the anisotropy can be seen from Fig. 5, which shows $j_n^{(X)}/j_n^{(O)}$ vs y_n for $n = 2$, $\gamma = 1.36$. The function is monotonic in y_n so the ratio uniquely determines the pitch angle. An isotropic distribution would have a ratio of 10.66 in this case or a weighted pitch angle of 67.2°. A polarization ratio larger than 10.66 indicates that the pitch angle distribution at this energy favors the perpendicular direction. A polarization ratio smaller than 10.66 implies that the distribution favors the parallel direction. The measured ratio of 2.82 gives a weighted pitch angle of 33.3°, showing the distribution is extended in the parallel direction as expected for LHCD. Using the uncertainty in the calibration gives error bars of ~4° for the weighted pitch angle. The other important feature in Fig. 5 is the minimum ratio. The limiting value of the ratio as the distribution becomes beamlike is $\gamma^2/(\gamma^2-1)$. Referring back to the assumption that the high-frequency peak in the spectra is due to third-harmonic emission, the polarization ratios in that peak are smaller than the theoretical minimum for second-harmonic emission at those frequencies. This further validates the assignment of this emission to the third harmonic.

The pitch angle analysis is repeated for each of the frequencies. The results are plotted in Fig. 6, where the distance from the origin is the resonant momentum and the pitch angle is given by the analysis. Also plotted on this graph are the limits of the interaction region of the main lobe of the LH power spectrum. The curved lines are these limits corrected for relativity. Wave accessibility limits the maximum paral-

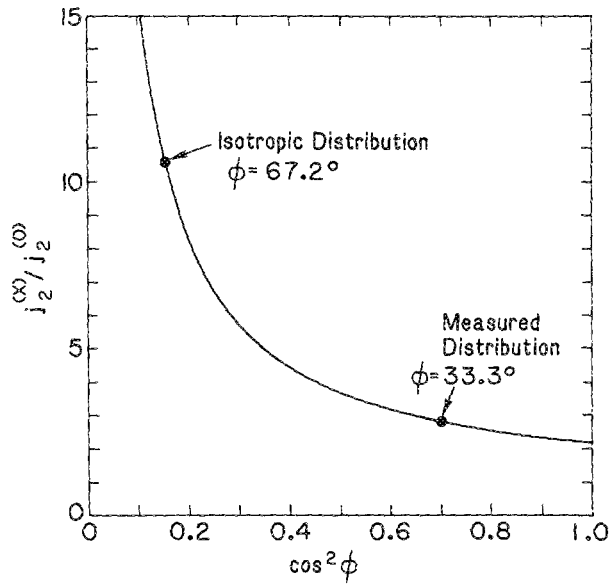

FIG. 5. Plot of the polarization ratio versus pitch angle for the case $n = 2$ and $\gamma = 1.36$.

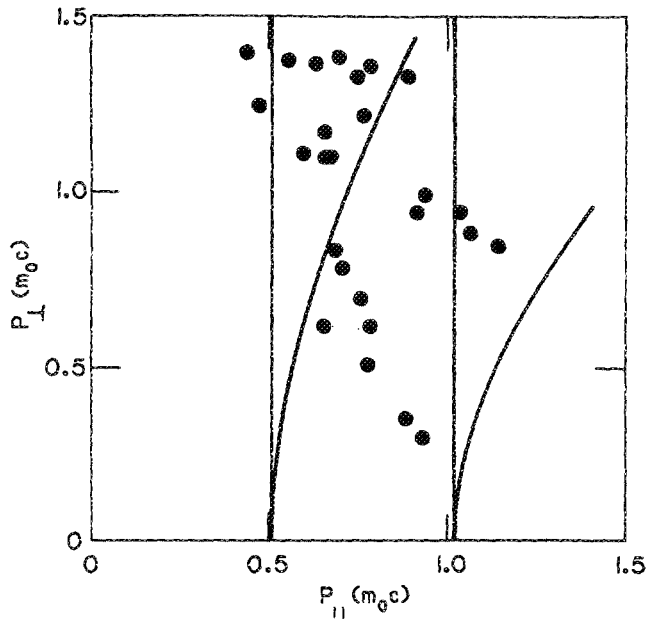

FIG. 6. Pitch angle distribution given by the transformation for a steady-state LHCD discharge.

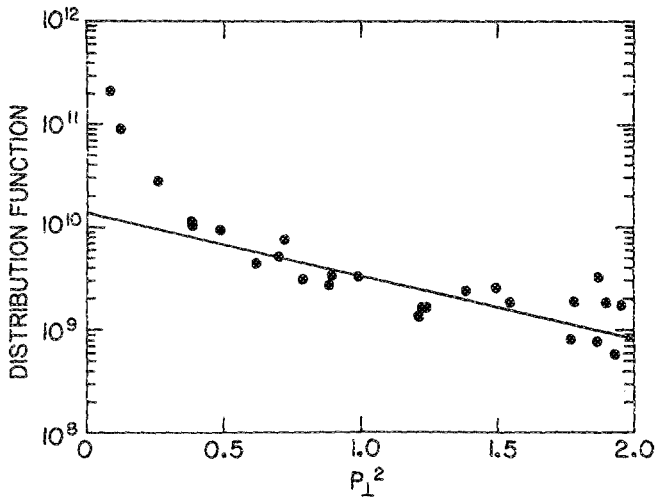

FIG. 7. Distribution function inferred from the transformation plotted against $p_\perp^2$.

lel velocity where the LH waves can interact with electrons. Since there is no loop voltage at the time these spectra were taken, the electric field is assumed to be much too small to generate runaways. Therefore particles are not expected to be in front of this interaction region on the average. The figure indicates that the electrons are, on the average, where they are expected to be—in or behind the main interactions region.

A few more assumptions are necessary to determine ρ from the calibrated emission. The quantity j_n must be integrated over frequency, solid angle, and volume to model the power received by the radiometer. The frequency integral is performed by assuming j_n is constant in ω over the bandwidth of the instrument. To integrate over solid angle, the emission is taken to be independent of the observation angle as the angle is varied over 2.5° around the central angle. The volume integral is performed by assuming the velocity distribution is independent of position. The emitting volume is taken to be a cylinder with a radius of 2.5 cm (the measured width of the antenna pattern at the plasma center) and length of $\pm$ 20 cm. The value of 20 cm was chosen by examining the Abel-inverted profiles from perpendicular-viewing hard-x-ray bremsstrahlung. The x-ray emission drops to a factor of 10 below its peak value at $\pm$ 20 cm. Taking the velocity distribution to be independent of position is the least justified of all the assumptions because there is little evidence to support or refute it. However, this does not preclude drawing conclusions about the distribution provided one considers ρ and y_n to be line-averaged quantities. Since the points in Fig. 6 fall in a narrow range of values of $p_\parallel$, the distribution is plotted against $p_\perp^2$ (see Fig. 7) to indicate an effective perpendicular temperature. The line shown is a least-squares fit to the points, omitting the three points at low $p_\perp^2$. The temperature implied is 180 keV. The three points at low $p_\perp^2$ are consistent with a perpendicular temperature of 35 keV. Knowing the perpendicular distribution, the self-absorption of the superthermal electrons can be calculated. An estimate of the optical depth is given[12] by $\tau = T_{\rm rad}/T_\perp$, where $T_{\rm rad}$ is the radiation temperature (see Fig. 4). By this method, the maximum O-mode optical depth is $\sim$0.06 and the maximum X-mode optical depth is $\sim$0.14. An optical depth of 0.14 corresponds to 7% absorption. Therefore, negligible absorption is a self-consistent assumption.

The transformation analysis presented has two advantages over the transformation technique introduced by Kato and Hutchinson.[7] The previous technique measured the anisotropy by fitting the data to an analytic function which places the maximum of the pitch angle distribution at $y = 0$ or 1. This form is sufficient for runaway discharges. However, for LHCD discharges where electrons have total momentum greater than the wave accessibility limit on parallel momentum, the peak of the pitch angle distribution at these energies is at some pitch angle between 0° and 90°. This would also be the case for distributions during electron cyclotron resonance heating experiments relying on Doppler-shifted absorption. The technique presented here is valid for all one-sided discharges. The second advantage is that the technique described here lends itself naturally to a display of the distribution function dynamics. This is illustrated by showing three cases where the critical energy for the runaway of electrons is altered by varying the density and electric field. The details of this experiment are discussed elsewhere[13,14]; only the conclusions will be presented here as a demonstration of the technique. Figure 8 shows three comparisons. In each case the open circles are for a steady-state LHCD discharge where the LH waves do not directly populate the runaway region. The critical energy for runaway is given by balancing the electric field force against collisional drag.[15] The effects of particle acceleration will be seen in the pitch angle plot—points above the critical energy should move to smaller pitch angles (more anisotropic in the parallel direction) and points below the critical energy should move to larger pitch angle (up to the point indicating an

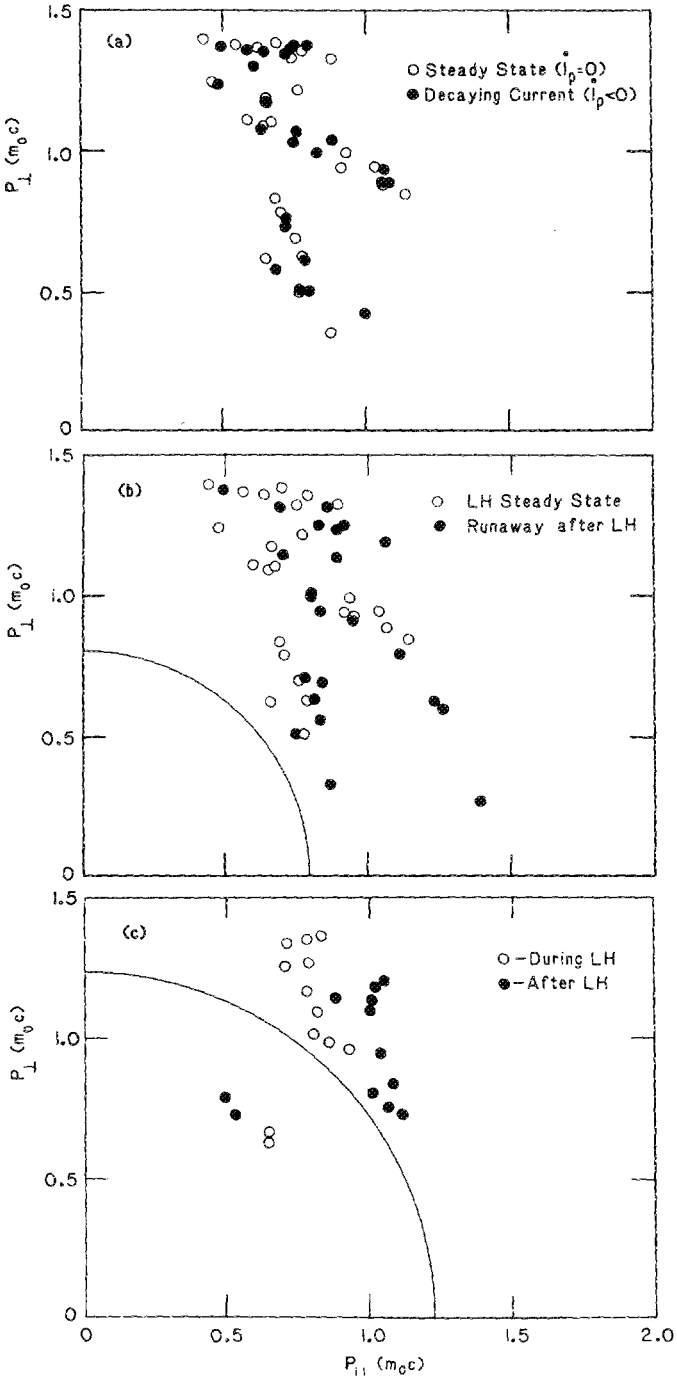

FIG. 8. Comparisons of pitch angle distributions for three different values of critical runaway energy. In each case the open circles are a steady-state LHCD discharge with no runaway. The closed circles are discharges where the runaway boundary is (a) 800, (b) 140, and (c) 250 keV. The boundary is plotted for cases (b) and (c).

isotropic distribution). In Fig. 8(a), the closed circles are for a discharge where the electric field is only slightly raised. The critical energy is 800 keV and no evidence of electron acceleration is seen. In Fig. 8(b), the closed circles are for a discharge where the electric field is raised and the density lowered from the reference case. The critical energy is now 140 keV (the circular boundary on the graph) and all energies show evidence of acceleration. Finally, in Fig. 8(c), both the electric field and density are higher. The critical energy is now 250 keV. The points above this energy indicate that the electrons are running away, while the points below this energy indicate that the distribution is becoming more isotropic.

III. CONCLUSIONS

We have presented a diagnostic technique for measuring superthermal distributions with good energy and time resolution. The experimental arrangement permits a direct connection between particle energy and emission frequency when the emission can be assigned to one harmonic. A transformation was formulated which allows interpretation of the emission in the X- and O-mode polarizations in terms of the anisotropy and number density of the distribution at each energy. This transformation was applied to steady-state LHCD discharges; the resulting distributions were consistent with theoretical predictions and previous measurements. The technique also illustrates the dynamics of the superthermal distribution as demonstrated by the example of varying the runaway boundary. The main limitations of the technique are that the expected distribution should be one sided and the information obtained is line averaged rather than local.

[a] Present address: General Atomics, San Diego, CA 92138.

[1] N. J. Fisch, Rev. Mod. Phys. **59**, 175 (1987).
[2] B. W. Stallard *et al.*, *Applications of Radio-Frequency Power to Plasmas*, AIP Conference Proceedings No. 159 (AIP, New York, 1987), p. 21.
[3] C. M. Celata and D. A. Boyd, Nucl. Fusion **17**, 735 (1977).
[4] S. Tamor, Nucl. Fusion **19**, 455 (1979).
[5] K. Kato and I. H. Hutchinson, Phys. Fluids **30**, 3809 (1987).
[6] I. H. Hutchinson, K. Kato, and S. C. Texter, Rev. Sci. Instrum. **57**, 1951 (1986).
[7] K. Kato and I. H. Hutchinson, Phys. Rev. Lett. **56**, 340 (1986).
[8] G. Bekefi, *Radiation Processes in Plasmas* (Wiley, New York, 1966).
[9] J. Fischer, J. Benson, and D. A. Boyd, Int. J. Infrared Millimeter Waves **4**, 591 (1983).
[10] P. C. Efthimion, V. Arunasalam, R. Bitzer, L. Campbell, and J. C. Hosea, Rev. Sci. Instrum. **50**, 949 (1979).
[11] G. Taylor *et al.*, Rev. Sci. Instrum. **55**, 1739 (1984).
[12] G. Giruzzi, I. Fidone, G. Granata, and R. L. Meyer, Phys. Fluids **27**, 1704 (1984).
[13] T. C. Luce, P. C. Efthimion, and N. J. Fisch, Phys. Rev. Lett. (to be published).
[14] T. C. Luce, Ph.D. dissertation, Princeton University, 1987.
[15] C. W. Barnes, Ph.D. dissertation, Princeton University, 1981.